Confined ion energy >200 keV and increased fusion yield in a DPF with monolithic tungsten electrodes and pre-ionization

Cite as: Phys. Plasmas **24**, 102708 (2017); https://doi.org/10.1063/1.4989859
Submitted: 12 June 2017 • Accepted: 04 October 2017 • Published Online: 20 October 2017

Eric J. Lerner, Syed M. Hassan, Ivana Karamitsos, et al.

Confined ion energy >200 keV and increased fusion yield in a DPF with monolithic tungsten electrodes and pre-ionization

Eric J. Lerner, Syed M. Hassan, Ivana Karamitsos, and Fred Von Roessel
LPP Fusion, Inc., Middlesex, New Jersey 08846, USA

(Received 12 June 2017; accepted 4 October 2017; published online 20 October 2017)

To reduce impurities in the dense plasma focus FF-1 device, we used monolithic tungsten electrodes with pre-ionization. With this new set-up, we demonstrated a three-fold reduction of impurities by mass and a ten-fold reduction by ion number. FF-1 produced a 50% increase in fusion yield over our previous copper electrodes, both for a single shot and for a mean of ten consecutive shots with the same conditions. These results represent a doubling of fusion yield as compared with any other plasma focus device with the same 60 kJ energy input. In addition, FF-1 produced a new single-shot record of 240 ± 20 keV for mean ion energy, a record for any confined fusion plasma, using any device, and a 50% improvement in ten-shot mean ion energy. With a deuterium-nitrogen mix and corona-discharge pre-ionization, we were also able to reduce the standard deviation in the fusion yield to about 15%, a four-fold reduction over the copper-electrode results. We intend to further reduce impurities with new experiments using microwave treatment of tungsten electrodes, followed by the use of beryllium electrodes. *Published by AIP Publishing.*
https://doi.org/10.1063/1.4989859

I. INTRODUCTION—THE DENSE PLASMA FOCUS (DPF) DEVICE

DPF is a compact and simply constructed device first developed in the 1960s by N. V. Filippov in the USSR and by J. W. Mather in the United States and has been studied by dozens of groups over the last 50 years, resulting in a large and rich literature. It consists of two concentric cylindrical electrodes enclosed in a vacuum chamber. The chamber is evacuated to low pressure and then backfilled to several Torr with the fuel gas. A pulse of electricity with a rise time of 0.2–10 μs from a capacitor bank is discharged across the electrodes during operation.[1] In operation, as the capacitors discharge, the gas is ionized and a current sheath, often consisting of pinched current filaments,[2,3] forms and runs down the electrodes. When the sheath reaches the end of the inner electrode (the anode), the filaments pinch together in the center, forming dense, magnetically confined hot spots or plasmoids.[4,5] The plasmoids emit X-rays with energies from several keV to over 100 keV. X-ray pinhole images have demonstrated that the plasmoids can be tiny, with radii of hundreds of microns or less.[6–9] The plasmoids can have densities in the range of 10^{20}–10^{21} cm^{-3}. These densities were measured by a number of independent methods, including heavy ion and secondary product fusion,[10,11] CO_2 laser scattering,[12] and X-ray line intensities.[13] These plasmoids emit intense beams of accelerated ions and electrons.[14–18] Neutrons from fusion reactions are emitted from the device in large quantities (up to 10^{13}) per shot.

II. ANALYSIS OF IMPURITY EFFECTS

There is good evidence that heavy-metal impurities limit the fusion yield in mega-ampere plasma focus devices.[19] Such impurities decrease the conductivity of the plasma in the current-carrying sheath, leading to disruption of current filaments through over-heating.[20] The elimination of the filaments, combined with enhanced radiation from the impurities, limits the density in the current sheath. This in turn leads to lower plasma density and thus lower fusion yield in the plasmoid that forms during the focus phase. In addition, the disruption of the highly magnetized filaments allows the formation of additional current sheaths, draining energy from the plasmoid and further reducing fusion yield. Third, the unequal distribution of impurities leads to asymmetric compression, also reducing density and yield.

We can calculate approximately the amount of impurity of a given element that is required to disrupt the filaments. A heated plasma moves into a cool plasma or neutral gas in a way that minimizes the total dissipation of energy. The two principal ways energy is dissipated from the current sheath in a plasma focus device are through electrical resistance of the current moving through the sheath and through hydrodynamic friction of the sheath moving through the background medium. Electrical resistance is minimized by an even distribution of current, but hydrodynamic friction is minimized by filamentation—the balance between the two processes determines if filamentation will occur.

Hydrodynamic dissipation power is

$$P_F = 0.5\, n_a v_A^3 r_f L N \mu M_p \ (\text{ergs/s}), \tag{1}$$

where v_A is the Alfven velocity of the current sheath, M_p is the mass of a proton, μ is the mean atomic mass, n_a is the fill gas particle density, and N, r_f, and L are the filaments number, radius, and length, respectively.

Electrical resistive dissipation power is

$$P_r = \frac{1}{2} \cdot \frac{\eta L I^2}{N \pi r_f^2} \left(\frac{\text{ergs}}{\text{s}}\right), \tag{2}$$

where η is the electrical resistivity, and I the total current in statamperes.

The sum of the two terms will be minimized for

$$r_f^3 = \frac{4\,\eta I^2}{N^2 \pi n_a v_A^3 \mu M_p}\ (\mathrm{cm}^3). \tag{3}$$

It will be difficult for filaments to form unless $r_f < \pi r_a/2\,N$, where r_a is the anode radius, so

$$r_a^3 > \frac{32\,\eta N I^2}{\pi^4 n_a v_A^3 \mu M_p}\ (\mathrm{cm}^3). \tag{4}$$

Since

$$I^2 = \pi r_a^2 n_a v_A^2 c^2 \mu M_p, \tag{5}$$

we then have

$$r_a > \frac{32\eta N c^2}{\pi^3 v_A}(\mathrm{cm}). \tag{6}$$

This can be interpreted as a lower limit on the magnetic Reynolds number

$$R_m = \frac{4\pi r_a v_A}{\eta c^2}, \tag{7}$$

$$R_m > 128N/\pi^2, \tag{8}$$

if we take the linear dimension as r_a. If we instead take the linear dimensions as r_f,

$$R_m > 64/\pi. \tag{9}$$

So, to form vortices, the flow velocity must be considerably larger than the magnetic diffusion velocity on the scale of the filament radius.

To see the effects of impurities, we can write the resistivity, η, as

$$\eta = \frac{2\sqrt{2\pi}\, e^2 f z_i^2 \sqrt{m_e}\, ln\Lambda}{3\,(kT_e)^{3/2}}, \tag{10}$$

where f is the fraction of ions with charge z_i, T_e is electron temperature in eV, I the total current in A, and z is the ratio of electron-to-ion density.

We can approximately assume that magnetic and thermal pressure are balanced in the sheath, so

$$kT_e = \frac{1}{2}\cdot\frac{\mu M_p v_A^2}{(z+1)}. \tag{11}$$

Combining (10) and (11)

$$\eta = \left(\frac{8\sqrt{\pi}\, e^2 f z_i^2 ln\Lambda}{3 z M_p v_A^3}\right)\left(\mu/(z+1)\right)^{-\frac{3}{2}}\left(\frac{m_e}{M_p}\right)^{\frac{1}{2}}. \tag{12}$$

We can then use (6) to produce a dimensionless criterion for filament formation and a limit on impurity

$$f z_i^2 < \left(\frac{3}{256}\right)\pi^{\frac{5}{2}}\left((z+1)/\mu\right)^{-\frac{3}{2}}\left(\frac{M_p}{m_e}\right)^{\frac{3}{2}}\left(\frac{r_a}{r_e}\right)\left(\frac{z\beta^4}{N ln\Lambda}\right), \tag{13}$$

$$= 7\times 10^{-26} r_a z v_A^4\left((z+1)/\mu\right)^{-\frac{3}{2}}\left(\frac{1}{N ln\Lambda}\right), \tag{14}$$

where r_e is the classical radius of the electron and β is v_A/c.

We can take as an example the conditions in FF-1 at the end of the run-down phase with $v_A = 1.1 \times 10^7$ cm/s, $r_a = 2.8$ cm, and deuterium fill pressure 20 Torr. With 16 cathode vanes, we take the minimum N to be 32, as the filaments will tend to form in counter-rotating pairs. Then, $f_c z_i^2 < 11$, where f_c is the critical concentration above which we expect no filamentation. For tungsten impurities this would put the limit at 20% by mass. So, with impurity above this level, it is unlikely that filamentation will exist at the end of the run-down.

By comparison with our previous results, in 2013 we ran FF-1 with a cathode consisting of 14-cm long cylindrical Cu rods screwed into a tungsten plate and a 2.8 cm radius Cu anode that was plated with Ag. We estimated[19] in these experiments an impurity level of about 50% of the deuterium mass. If this was about half Cu and half Ag then $f z_i^2 = 17$. In this case, our theory would predict no filaments survive to the end of run-down, which is what we observed.

If we want to be sure that the filaments can form (or reform if disrupted) before the end of the run-down, we have to require an impurity fraction f that is low enough so that filamentation begins adequately early in the run-down. While typical filamentation growth times of the order of r_f/v_A are much shorter than the rundown-time, we can conservatively require that the sheath be unstable to filamentation no later than half-way through the rundown time. At this point v_A will be approximately 0.7 times the peak value at the end of the run-down.

Assuming the source of the impurity is at the start of the run-down (as is shown in Sec. III) the fraction f_c will be higher in the earlier phases of the rundown, roughly in inverse proportion to the distance the sheath has traveled, which in turn is roughly proportional to v_A^2. Therefore f at the end of run-down is inversely proportional to v_A^6, and thus is about $f_c/8$, so in this case $f_c\, z_i^2 < 1.4$.

We can thus approximately distinguish a low-impurity regime with $f\, z_i^2 < 1.4$, where we expect filaments to be present at the end of run-down and a high-impurity regime, $f z_i^2 > 11$, where filaments will almost certainly not be present, with an intermediate impurity regime in between, where filamentation is uncertain.

III. SOURCES OF IMPURITY

Two primary sources of impurities are vaporization of electrode metal from arcing between separate pieces of the electrodes and vaporization of the anode by runaway electrons during the initial breakdown of the plasma.[19] In order to eliminate the first source, we installed monolithic electrodes in the FF-1 device in 2015. These electrodes are single pieces, connected to the rest of the circuit outside the vacuum chamber, so no arcing vaporization is possible. To provide mechanical rigidity to the cathode, the usual rods are replaced by vanes (Fig. 1). To reduce the second source, we changed the material of the electrodes from copper to tungsten, which is more heat-resistant. In addition, we implemented a pre-ionization procedure, so as to reduce the

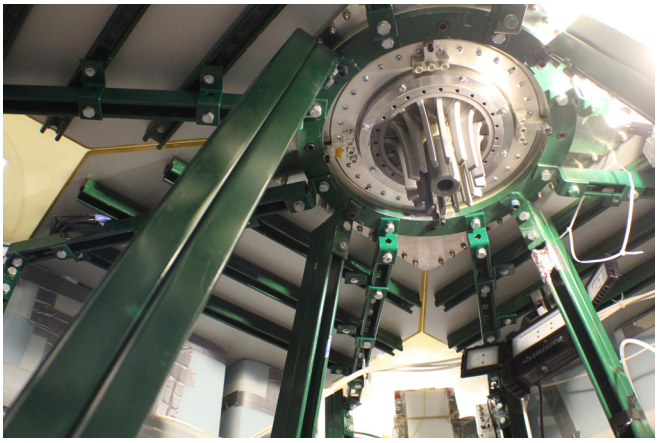

FIG. 1. Monolithic tungsten cathode and anode installed on FF-1. Vanes have replaced the standard rods in the cathode.

energy of the electrons in the main discharge. Pre-ionization has been used successfully with the DPF by several groups of researchers.[21–25]

Initial tests of the new electrodes in 2015 demonstrated the sensitivity of tungsten to oxide contamination. In the presence of heated deuterium, tungsten oxide reacts to form hydrogen tungsten bronze (H_xWO_3). While tungsten is highly heat-resistant, tungsten bronze easily dissociates starting at 500 °C.[26] Also, both tungsten bronze and tungsten oxide have low thermal and electrical conductivity, so heat up rapidly when exposed to high current density. We observed the production of characteristically golden-colored tungsten bronze layers on the electrodes and inner vacuum chamber surfaces, leading to high levels of tungsten impurities in the plasma.

We identified the main sources of oxygen as water vapor outgassing from silicone gaskets and other surfaces, and release of oxygen from chromium oxide layers in the stainless steel vacuum chamber. To reduce these sources, we had the vacuum chamber coated with 4 μm of TiN, and we baked-out the chamber and electrodes under vacuum for two weeks at a temperature of 120 °C. The virtual leak rate from outgassing was reduced from 12 to 1.3 μTorr per minute.

Finally, we doubled the length of the vacuum chamber by moving the floor of the chamber from 15 cm from the anode to 45 cm away in order to eliminate the splash-back onto the electrodes of material eroded from the tip of the anode near the pinch region.

Unfortunately, we did not succeed in entirely eliminating oxides due to a faulty valve introducing some trapped water vapor and to possible oxide formation during the bake-out itself. However, the oxides were unquestionably reduced as evidenced by a substantial reduction in the amount of colored tungsten bronze deposits.

IV. EXPERIMENTAL SET-UP

In testing the pre-ionization, we initially used a shunt resistor from the capacitor charging circuit. We ran a series of shots with pure deuterium using this set-up. However, we found this led to a series of arc breakdowns, often concentrated in a single region of the anode. Despite the small current involved, about 100 A, we observed that these arcs could produce tungsten dust, so were still able to vaporize the tungsten oxides. In addition, the exact conditions of pre-ionization at the time the main current turned on were not constant from shot to shot. To avoid this effect, we switched to a separate pre-ionization circuit with an adjustable high-voltage power supply providing microampere currents through a 1.25 GΩ resistance (Fig. 2). With pure deuterium, we found that we could not achieve a steady, corona-discharge pre-ionization (CDP). We were then able to get a steady corona discharge for pre-ionization with a deuterium-nitrogen mix with N > 3% by volume. However, we were only able to achieve a pinch with fusion yields for N < 6%. Within this range, the best performance was consistently obtained 4.4%–4.8% N.

We fired a bank of eight capacitors with a total of 75 μF capacitance charged to 40 kV, for a bank energy of 60 kJ. This produced a 1.2 MA peak current with a rise time of about 1.8 μs. The anode and cathode have the same length, 14 cm, with anode outer radius being 2.8 cm and the 16 vanes of the cathode touching a circle with radius 5 cm. They are separated by an alumina insulator with a length of 2.8 cm.

V. RESULTS

A. Reduction in impurity

We found evidence that the new conditions did indeed reduce the erosion from the anode near the insulator. First, the dip in current that occurred during the first 100 ns of the current rise was substantially reduced in the new shots relative to those with copper electrodes and no pre-ionization (Fig. 3). On average, the total energy lost in these dips declined by 50% with the new conditions as compared to the old, which clearly reflected a reduction in energy absorbed by vaporization and ionization of material from the anode surface.

This was confirmed following the firing run by direct examination of the anode. During a 125-shot run with silver-coated copper anode, an easily measurable reduction of over 200 μm was observed in the anode diameter in the 0.8 mm wide region near the insulator. No such reduction was measurable with a 150-shot run with the tungsten anode, putting an upper limit on the erosion of about 25 μm. In addition, we

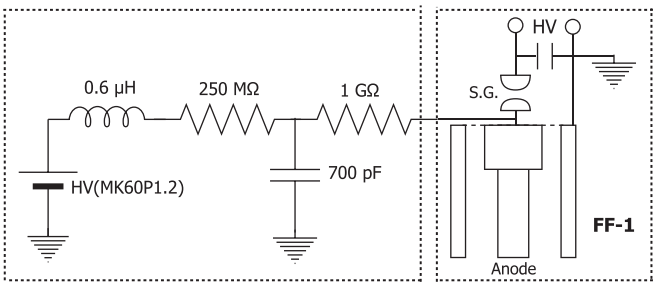

FIG. 2. Pre-ionization circuit connects an adjustable high-voltage power source (max 60 kV) to the central anode of FF-1 through a 1.25 GΩ resistance. To protect the power supply during the shot, we included an inductor coil and capacitor.

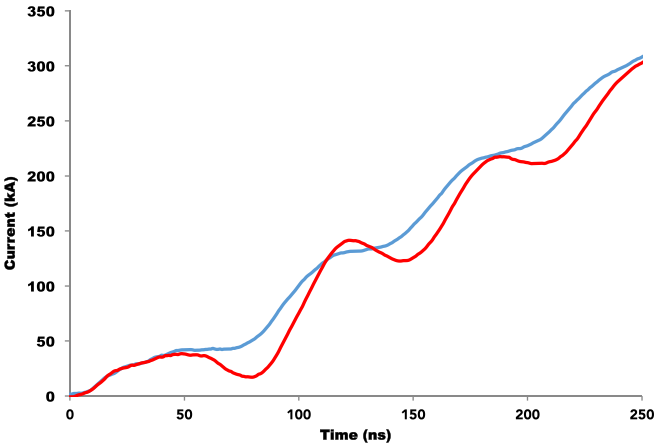

FIG. 3. The early dip in current at about 70 ns after pulse initiation is greatly reduced with tungsten electrodes and pre-ionization (upper curve) as compared to copper electrodes and no pre-ionization (lower curve).

used a Fourier analysis of audio produced by rubbing the two anode surfaces near the insulator. This showed a roughly 3-fold reduction in roughness at long (100-μm) wavelengths for tungsten relative to copper, again confirming a substantial reduction in erosion.

We also measured a reduction in the effect of impurities on the speed of the run-down phase. Using S. Lee's simulation model,[27] shots from both the copper-electrode shots and the tungsten anode shots were fitted, allowing the external inductance to be varied in the simulations. We had previously measured the external inductance of the circuit using high-pressure N shots to be 26 nH. However, to fit the copper electrode results, the simulation inductance had to be increased to 40 nH, while the tungsten result could be fit with an external inductance of 30–32 nH.

These results are consistent with a reduction in impurity mass by about a factor of three and thus a factor of 10 reduction in impurity by ion number, given the mass ratio of tungsten to copper. Due to tungsten's greater z, the reduction of the fz^2 factor is then from about 17 to 9, thus moving only from the high to medium impurity level.

This is for a typical shot in the tungsten series. It is more difficult to estimate the range of impurity. The near-UV spectra showed tungsten lines that were quite consistent from shot to shot as measured as a fraction of the continuum intensity. The minimum-intensity lines were only about 10% less than the mean. But the variability of run-down time, discussed below, indicated a wider range of impurity, with the minimum calculated impurity values roughly 60% below the mean. The Lee simulation fits indicate an intermediate minimum value of about 35% below the mean.

The contribution of tungsten oxides to the plasma was clearly evidenced in the optical-NIR spectra obtained from slits pointed at the anode above the region of the pinch. These showed a clear peak at 777 nm, typical of oxygen.

B. Energy transfer and fusion yield

The reduction in impurity was accompanied with an improvement in conditions at the pinch. The "early beam," an increase in current immediately before the strong decrease in current at the time of the pinch, had been observed consistently with the copper electrodes.[2] However, this phenomenon was essentially eliminated with the tungsten electrodes.

We used both pure deuterium and deuterium-nitrogen fill gases. With the first shots with pure D and arcing pre-ionization, we achieved a 56% increase in best-shot fusion yield compared with the previous copper electrodes, to 2.5 $\times 10^{11}$ neutrons. We also increased mean yield for a sequence of 10 shots by 66% to 1.5 $\times 10^{11}$ neutrons (see Table I). For comparison, the peak yield was 50% higher than the yield of any other plasma focus device at 1.2 MA and double the yield of any other PF for a bank energy of 60 kJ. See Herold *et al.* for comparison values from other researchers.[28]

Using D-N mix and corona-discharge pre-ionization, we almost matched the increase in mean yield for pure D, increasing this by 56%, although we did not match the increase in single-shot yield.

In addition, very significantly, with corona-discharge pre-ionization (CDP) we observed a four-fold decrease in shot-to-shot variability over a ten-shot run as compared with copper electrodes and nearly 3-fold reduction as compared with the pure D results with arcing pre-ionization. These results are quite similar to those obtained using pre-ionization with much smaller-current PF devices. The large reduction in variability strongly indicates that much of the well-known shot-to-shot variability in PF devices is due to unsymmetrical breakdown, which pre-ionization greatly reduces.[23]

The D-N, CDP shots also produced a 40% increase in mean ion energy for a single shot (June 7, 2016, shot 6), to a record of 240 ± 20 keV for any PF device. This is a record

TABLE I. Results are compared between copper electrodes, tungsten with pure D, and tungsten with D-N mix with and without corona discharge pre-ionization. Mean values are shown for the best ten-shot sequence. Statistically significant (at 1% level) differences from the copper results are shown in bold and results obtained outside the ten-shot sequences are shown in parentheses.

Electrodes material (condition)	Gas	Total pressure (Torr)	Number of shots	Neutron yield (single-shot) $\times 10^{11}$	Neutron yield (mean 10 shots) $\times 10^{11}$	Neutron Yield s.d. (%)	Mean ion energy (single-shot) keV	Mean ion energy (mean 10 shots) keV
Copper	D_2	24	10	1.6	0.9	55	135 (170)	77
Tungsten	D_2	18-20	8	**2.5**	**1.5**	38	200	71
Tungsten (No Pre-ionization)	$D_2 + N_2$	18	7	1.9	1	41	124	78
Tungsten (Pre-ionization)	$D_2 + N_2$	18	10	1.7	**1.4**	**14**	**225 (240)**	**124**

for confined ion energy in any fusion-fuel plasma using any device. A second shot (June 2, 2016 shot 8) was measured with E_i of 225 keV. We observed as well a 61% increase over the best copper results in E_i averaged over 10 consecutive shots with the same conditions.

These results exceeded a previously reported record in 2012 of 170 keV for confined mean ion energy in the same PF device with copper electrodes.[29] It also exceeded the 100–200 keV gyrating ions reported by Kubes *et al.* in 2015.[30]

We measured mean ion energy E_i by time-of flight measurements of neutrons at 11 m and 17 m from the device axis. The TOF PMTs were located at the height of the end of the anode, perpendicular to the machine axis. They had a collimated field of view of only 2 cm vertically from the tip of the anode. As described previously,[7] the spread in neutron velocities in the perpendicular direction must be due to high-energy ions which are confined within the central plasmoid produced at the tip of the anode (Fig. 4). The duration of the neutron production, measured both by projecting back the TOF signals and by a third PMT located at 1.34 m, is 40 ns, and the neutron yield was 1.6×10^{11}.

In these shots, as in previous work[30] with FF-1, the neutrons observed cannot be mainly produced by an axial beam passing through either a dense plasmoid or through the background gas. Such a beam would produce a strong asymmetry in neutron distribution, with far more neutrons in the axial, down-beam direction than horizontally. We observed no such large asymmetry.

Comparing neutron measurements by cross-calibrated bubble detectors at 4° and 90° from the axis, we found an asymmetry for 10 shots of only 1.3 ± 0.1 towards the axial direction. By contrast, if the neutrons were produced by a beam interacting with the 1.6 m-long column of deuterium in the vacuum chamber and drift tube, we would expect more than 100 times as many neutrons at the 4° than at the 90° detector. Thus, only confined ions that are gyrating within the plasmoid, not moving in an axial beam, can produce the neutrons observed.

Of course, there is no reason to believe that these ions are Maxwellian in velocity distribution, and therefore we do not refer to the ion mean energy as a temperature. In a previous work,[29] we have calculated the density of the plasmoids as about 3×10^{19} cm^{-3} and for that density, 250 keV ions will take a few microseconds to thermalize, far longer than the 40 ns lifetime of the plasmoids.

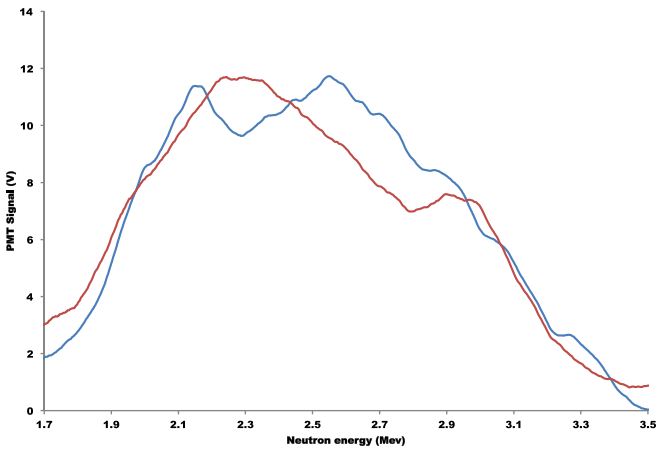

FIG. 4. PMT signals at 11.5 m (red) and 17.5 m (blue) plotted against neutron energy, determined by time of flight. The vertical scale of the NTF signal is expanded to match that of the FTF. There is good agreement with a FWHM of 1.16 ± 0.02 MeV for a mean ion energy of 240 keV.

On the other hand, there is also no evidence in our results for two populations of ions with widely different E_i. The distribution of neutron arrival times is sufficiently close to the expected Gaussian curve that we can exclude, for a wide range of hypothesized parameters, a relatively cold, dense background plasma colliding with a 500 keV fast ion population to produce collisions with 250 keV average energy. The colder ions would produce a central, sharply peaked distribution of neutron arrival times while the hot ions colliding with each other would produce greater-than Gaussian wings to the arrival time distribution. We observed neither. However, a very-low-energy background plasma within the plasmoid with $E_i < 7$ keV would produce too few neutrons to be observed, so we cannot exclude that possibility. Neither do we see any positive evidence for it.

For comparison, we performed 6 shots with no pre-ionization but with the same D-N mix. While the number of shots was limited, the mean fusion yield, yield variability, and E_i were essentially identical with that for the copper electrodes. The difference between mean fusion yield of the 10-shot pre-ionization run and the 7-shot no- pre-ionization run was significant at the 2 sigma level. For E_i, only the D-N CDP shots had significant increase over copper, with both the no-preionization D-N mix and arcing-preionization pure D having the same mean E_i as copper.

Energy transfer to the pinch also increased significantly from the copper to tungsten electrodes. The average voltage spike at the time of the pinch increased by 120% from 37 to 81 kV and the maximum spike for a single shot increased from 45% from 62 to 90 kV. Based on inductance calculations using the formulas of Bruzzone *et al.*,[31] we calculated that maximum energy transfer into the pinch increased to about 8 kJ. For energy transfer, there was no significant difference among the preionization and no-preionization conditions.

After the first 100 shots, which was after 50 shots with pinches, fusion yield began to deteriorate, reverting to about the same levels as copper electrodes by the time the series ended at 150 shots. The last shots showed a return as well of the early beam phenomenon and an increase in the early dips in current. While the reason for the decline is not determined, it seems likely that the increased roughening of the anode surface probably led to increasing asymmetry in breakdown and therefore in the current sheath and subsequent pinch.

C. Correlations of yield, E_i, and V with impurity

To further test the hypothesis that increases in fusion yield and E_i are due to decreases in impurity, we looked at correlations with run-down time. We expect the run-down time to vary inversely with fill pressure or, for a mix, with total gas mass density. We wanted to compensate for this dependence, so that the deviation from the expected run-

down time would be due to a greater or lesser mass of impurity. We found that for the range of pressures we used, the run-down time could be adequately fitted by a linear dependence on pressure of -34 ns/Torr D. We thus used an adjusted run-down time as a measure of impurity

$$t_a = t - 34.5(P_D + 7P_N), \tag{15}$$

where t_a is adjusted run-down time (ns), t is measured run-down time (time from start of pulse to maximum voltage), P_D is deuterium fill pressure in Torr, and P_N is nitrogen fill pressure.

As can be seen from Table II and Fig. 5, there are significant (at the 1% level) correlations of peak voltage and E_i on t_a for the entire sample of shots using tungsten. For yield (Fig. 6), the situation is somewhat more complex, as there are significant differences in the correlations for different conditions. The pure D shots and the early D-N mix shots share similar correlation, although the D-N mix has less scatter. But there is a significantly lower-yield for the later D-N mix shots, after shot 50.

D. Correlation of yield and pre-ionization level

We also tested the correlation of the pre-ionization with the yield. While the arcing pre-ionization conditions were not nearly as controllable as those with CDP, they did provide data that allowed us to see how yield varied with the ionization level achieved during pre-ionization.

In conditions where no runaway electrons are expected, the energy that an electron acquires between collisions with neutrals is just

$$E_e = Ee/n\sigma, \tag{16}$$

where E is the electric field, e the electron charge, n the neutral particle density, and σ the collision cross section of the neutrals.

We thus have

$$V_e = (2eE/mn\sigma)^{1/2}, \tag{17}$$

$$I = n_e v_e A e, \tag{18}$$

$$n_e = I/A(mn\sigma/2eE)^{1/2}, \tag{19}$$

where I is pre-ionization current right before the main breakdown, n_e is the electron particle density (equal to ion particle density), m is the electron mass, and A is the area of the current. If we assume A to be constant, we can observe the other variables for each shot. The current I was measured from the recorded drop of the anode voltage over the recorded time for the voltage drop

TABLE II. Analysis of shots.

Correlation	Sample	N	Slope	r
Log E_i on log t_a	all	48	−8.36	0.48
Log V on log t_a	all	48	−1.94	0.44

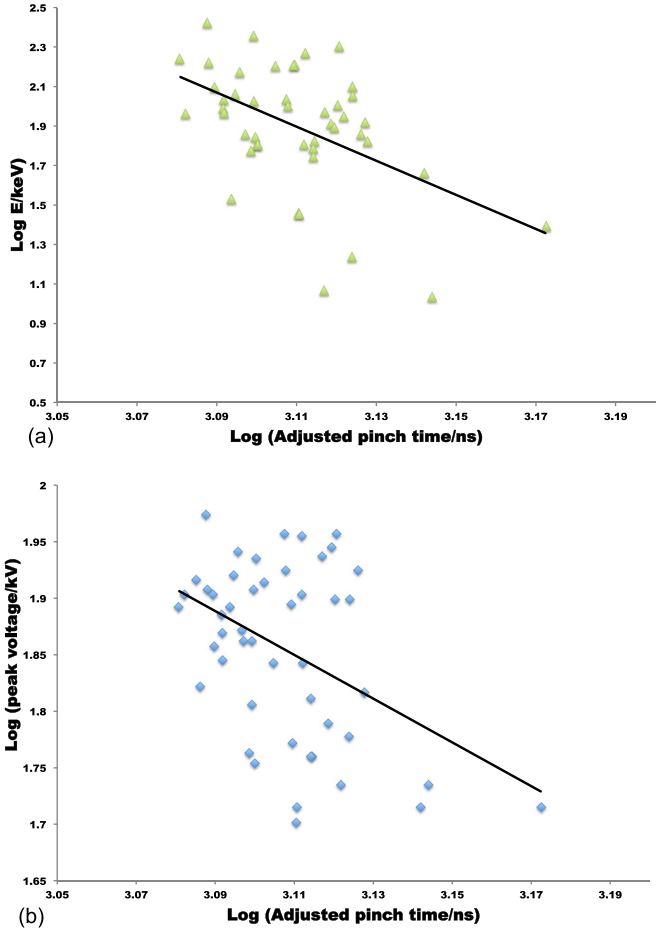

FIG. 5. Both the ion mean energy Ei and the peak voltage V show significant correlations with the adjusted pinch time. Lines show linear log-log fit to all shots.

$$I = \Delta V C_p/t_p. \tag{20}$$

ΔV is the voltage drop immediately before the main current rise (see Fig. 7), C_p is the capacitance of the plates changed during pre-ionization (which is a constant), and t_p is the time for the voltage drop.

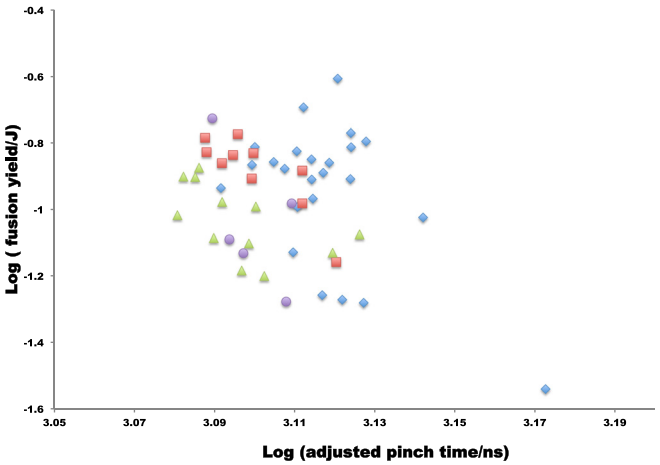

FIG. 6. Log fusion yield (J) plotted against log adjusted pinch time (ns). Pure D shots with arcing pre-ionization are blue trapezoids, D-N mix with CDP are red squares during first 50 pinches, green triangles during last 50 pinches. D-N mix with no pre-ionization are denoted as purple circles.

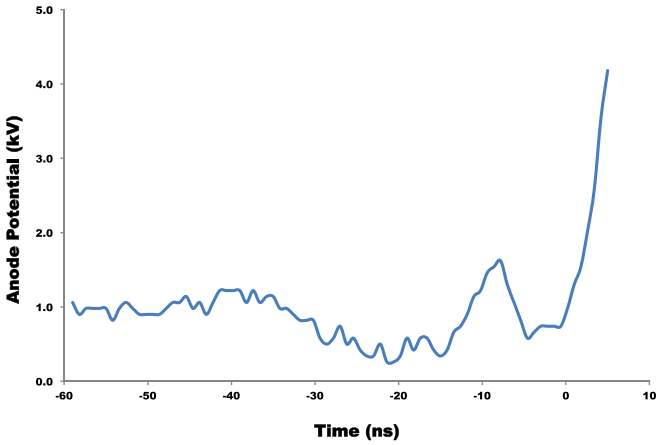

FIG. 7. Anode voltage (kV) vs time (ns) for shot 052316-01. Anode voltage drops sharply as pre-ionization charge breaks down across electrodes starting at –9 ns. This breakdown is used to calculate for each shot the current and thus the pre-ionization ion density right before the initiation of the main current beginning at time 0.

The resulting data, limited only to shots with fill pressure of 18 ± 2 Torr (Fig. 8), show a significant correlation at the 1% level between the calculated n_e and yield, with a near doubling of yield between the low and high end of the n_e range.

Of course correlation does not prove causation, and both higher yield and higher n_e could be due to a common cause, such as a smother anode surface leading to a more symmetrical breakdown. However, the significant decrease in yield without pre-ionization indicates that pre-ionization probably increases yield by allowing a more symmetrical initiation of the main current pulse.

There was no significant correlation of n_e with rundown time, so it seems unlikely that the effect of pre-ionization is, for these experiments, through a greater reduction of impurity.

VI. CONCLUSIONS AND PLANS FOR FURTHER EXPERIMENTS

Despite remaining impurities, the combination of tungsten electrodes and pre-ionization was able to demonstrate a three-fold reduction of impurities by mass and a 10-fold reduction by ion number. With the new set-up, FF-1 produced a 50% increase in fusion yield over the copper electrodes, both for a single shot and for a mean of ten consecutive shots with the same conditions. These results represent a doubling of fusion yield as compared with any other plasma focus devices with the same 60 kJ energy input. In addition, the device produced a new single shot record of 240 keV for mean ion energy, higher than for any other confined fusion plasma, and a 50% improvement in ten-shot mean ion energy. With a deuterium-nitrogen mix and corona-discharge pre-ionization, we were also able to reduce the standard deviation in the fusion yield to about 15%, a four-fold reduction over the copper-electrode results.

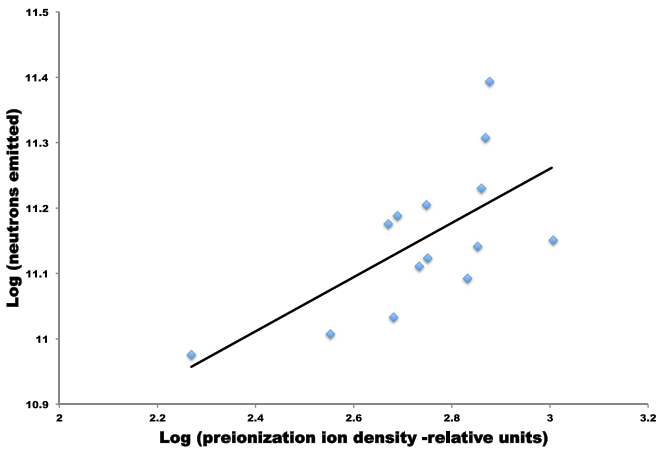

FIG. 8. For the arcing pre-ionization shots, there is a significant correlation of neutron yield with pre-ionization ion density, calculated as described in the text. Relative units are used to avoid uncertainties in the cross section of the current. The line shows the linear fit of the data, with a slope of 0.41, correlation $r = 0.65$ for $N = 13$.

These encouraging results were accompanied by the disappearance of the early beam phenomena and a concurrent doubling of the mean energy deposited in the pinch region, and a 45% increase in the single-shot deposited energy, as measured by the spike in the voltage at the time of the pinch. This improved efficiency in energy transfer to the pinch is, in our view, the likely immediate cause of the improved yield and E_i, although we cannot yet demonstrate that conclusively.

The range of impurity values, around 0.0015 by number, that we calculate for these shots imply values of fz^2 within the range our theory predicts will probably not allow filament formation, and we saw no evidence that filaments actually were present in the later phases of the run-down. So we do not attribute the improvement in performance to the achievement of filamentation, which would have greatly increased plasmoid density. Rather, the results are most consistent with the more modest reduction in impurity leading to greater symmetry of the sheath, the elimination of the early beam and a more efficient transfer of energy into the pinch.

To achieve optimal results, impurities must be further reduced, to reach the "low impurity regime" defined in Sec. III. In new experiments with tungsten electrodes, we are using a microwave heating of flowing hydrogen gas to more effectively remove the oxides. Beyond these experiments, we plan in the near future to replace the tungsten electrodes with beryllium electrodes, which will entirely eliminate the problem of high-Z impurities by excluding high-Z materials.

ACKNOWLEDGMENTS

We thank LPP Fusion's shareholders and donors, who funded this work. We would also like to thank Anthony Ellis, Mark Klapheke, and Jonathan Klabacha for their assistance in the assembly of the tungsten cathode, as well as Jose Varela for assistance with data processing.

[1]W. H. Bostick, V. Nardi, and W. Prior, J. Plasma Phys. **8**, 7 (1972).
[2]P. Kubes, M. Paduch, J. Cikhardt, J. Kortanek, B. Cikhardtova, K. Rezac, D. Klir, J. Kravarik, and E. Zielinska, Phys. Plasmas **21**, 122706 (2014).
[3]L. Soto, C. Pavez, F. Castillo, F. Veloso, J. Moreno, and S. K. H. Auluck, Phys. Plasmas **21**, 072702 (2014).
[4]C. R. Haas, G. Herziger, R. Lebert, and R. Noll, in Proceedings of 3rd International Workshop on Plasma Focus (1983), p. 87.
[5]G. Herziger, R. Noll, K. Ruehl, K. Schmitt, L. Michel, and H. Krompholz, in *Proceedings of International Conference on Plasma Physics*, 2–3 July 1984 (Ecole Polytechnique Federal De Lausanne, Lausanne, 1984), p. 31.

[6]M. Sadowski, H. Herold, H. Schmidt, and M. Shakhatre, Phys. Lett. A **105**, 117 (1984).
[7]H. Schmidt, in Proceedings of 3rd International Workshop on Plasma Focus (1983), pp. 63–66.
[8]K. N. Koshelev, V. I. Krauz, N. G. Rehetniak, R. G. Salukvadze, Yu. V. Sidelnikov, and E. Yu. Khatiev, J. Phys. D: Appl. Phys. **21**, 1827 (1988).
[9]L. Bertalot, R. Deutsch, H. Herold, U. Jager, H. J. Kaeppeler, A. Mozer, T. Oppenlander, B. Ruckle, M. Sadowski, P. Schilling, and H. Schmidt, "Experiments on plasma focus dynamics, neutron production and ion emission," in *Proceedings of the International Conference on IAEA Plasma Physics and Controlled Nuclear Fusion*, Brussels, 1–10 July 1980 (IAEA, Vienna, 1980), p. 177.
[10]J. S. Brzosko, V. Nardi, J. R. Brzosko, and D. Goldstein, Phys. Lett. A **192**, 250 (1994).
[11]J. S. Brzosko, J. R. Brzosko, B. V. Robouch, and L. Ingrosso, Phys. Plasmas **2**, 1259 (1995).
[12]G. R. Neil and R. S. Post, Plasma Phys. **23**, 425 (1981).
[13]I. V. Volobuev, V. A. Gribkov, D. Denus, N. V. Kalachev, T. A. Kozlova, O. N. Krokhin, S. Sledzinski, S. A. Straratsev, and S. Czekaj, Sov. J. Plasma Phys. **14**, 401 (1988).
[14]V. Nardi, W. H. Bostick, J. Feugeas, and W. Prior, Phys. Rev. A **22**, 2211 (1980).
[15]K. Hirano, K. Shimoda, T. Yamamoto, M. Sato, K. Kobayashi, and H. Misaizu, in *Proceedings of the 11th Europe Conference Controlled Fusion and Plasma Physics*, Aachen, 5–9 September 1983 (European Physics Society, Geneva, 1983), p. 551.
[16]L. Jakubowski, M. Sadowski, and J. Zebrowksi, Nucl. Fusion **41**, 755 (2001).
[17]L. Bertalot, H. Herold, U. Jäger, A. Mozer, T. Oppenländer, M. Sadowski, and H. Schmidt, Phys. Lett. A **79**, 389 (1980).
[18]E. J. Lerner, Laser Part. Beams **4**(2), 193 (1986).
[19]E. J. Lerner and H. R. Yousefi, Phys. Plasmas **21**(10), 102706 (2014).
[20]E. J. Lerner, D. Shannon, F. Van Roessel, I. Karamitsos, and A. Blake, in *Proceedings of the ICPIG* (2013), see http://www.icpig2013.net/papers/547_1.pdf.
[21]E. Ruden, H. U. Rahman, A. Fisher, and N. Rostiker, J. Appl. Phys. **61**, 1311 (1987).
[22]S. Ahmad, M. Sadiq, M. Shafiq, A. Waheed, P. Lee, and M. Zakaullah, Plasma Sources Sci. Technol. **15**, 314 (2006).
[23]S. Ahmad, S. S. Hussain, M. Sadiq, M. Shafiq, A. Waheed, and M. Zakaullah, Plasma Phys. Controlled Fusion **48**, 745 (2006).
[24]H. U. Khan, M. Shafiq, and M. Zakaullah, Radiat. Eff. Defects Solids **168**, 10 (2013).
[25]D. Piriaei, H. R. Yousefi, T. D. Mahabadi, A. SalarElahi, and M. Ghoranneviss, Phys. Plasmas **24**, 082502 (2017).
[26]V. K. Alimov, B. Tyburska, M. Balden, S. Lindig, J. Roth, K. Isobe, and T. Yamanishi, J. Nucl. Mater. **409**, 27 (2011).
[27]S. Lee, J. Fusion Energy **33**(4), 319 (2014).
[28]H. Herold, A. Jerzykiewicz, M. Sadowski, and H. Schmidt, Nucl. Fusion **29**(8), 1255 (1989).
[29]E. J. Lerner, S. K. Murali, D. Shannon, A. M. Blake, and F. Van Roessel, Phys. Plasmas **19**, 032704 (2012).
[30]P. Kubes, M. Paduch, J. Cikhardt, B. Cikhardtova, K. Rezac, D. Klir, J. Kravarik, J. Kortanek, and E. Zielinska, Phys. Plasmas **22**, 062705 (2015).
[31]H. Bruzzone, H. N. Acuña, M. O. Barbaglia, M. M. Milanese, R. Miklaszewski, M. Paduch, E. Zielińska, and A. Clausse, IEEE Trans. Plasma Sci. **44**(6), 968 (2016).